



## Heterogeneity across neural populations: Its significance for the dynamics and functions of neural circuits

Roman Baravalle  and Fernando Montani <sup>\*</sup>

*Instituto de Física de La Plata (IFLP), Universidad Nacional de La Plata, CONICET CCT-La Plata (1900) La Plata, Argentina*



(Received 20 September 2020; revised 16 February 2021; accepted 18 March 2021; published 12 April 2021)

Neural populations show patterns of synchronous activity, as they share common correlated inputs. Neurons in the cortex that are connected by strong synapses cause rapid firing explosions. In addition, areas that are connected by weaker synapses have a slower dynamics and they can contribute to asymmetries in the input distributions. The aim of this work is to develop a neural model to investigate how the heterogeneities in the synaptic input distributions affect different levels of organizational activity in the brain dynamics. We analytically show how small changes in the correlation inputs can cause large changes in the interactions of the outputs that lead to a phase transition, demonstrating that a simple variation in the direction of a biased skewed distribution in the neuronal inputs can generate a transition of states in the firing rate, passing from spontaneous silence (“down state”) to an absolute spiking activity (“up state”). We present an exact quantification of the dynamics of the output variables, showing that when considering a biased skewed distribution in the inputs of neuronal population, the critical point is not in an asynchronous or synchronous state but rather at an intermediate value.

DOI: [10.1103/PhysRevE.103.042308](https://doi.org/10.1103/PhysRevE.103.042308)

### I. INTRODUCTION

Modern experimental methodologies provide exceptional insights into the shape and features of neural circuits in the brain [1–4]. Recent advances such as neuropixels open the possibility of reading the statistical behavior of the neural activity by studying large populations of neurons [5–10]. However, to understand the complex statistics contained within these data, challenging research using new methodologies of complex systems needs to be carried out [11].

Complex systems in neuroscience are one of the fastest growing fields as new analysis and modeling techniques are required to extract meaning from the vast amount of data produced by recent brain measurement technologies [2–10]. Investigating how neurons process information from sensory inputs and complete computations to perform direct cognitive tasks is one of the main objectives of researchers working in neuroscience. Understanding how information is transmitted in the brain is of fundamental importance for gaining further insights into how the brain works [12–16]. However, information processing is susceptible to the brain states and the dynamics of the functional circuits [17,18].

Many properties of cortical circuits, such as recurrent excitation loops as well as feedback and forward inhibition, redundancy, and degeneracy, create substrates for a wide dynamic range of nonlinear and skewed distributions in the neuronal inputs [18–23]. Importantly, we still lack a proper theoretical framework, when considering the heterogeneities of the neuronal inputs, to investigate the nonlinear statistical emergent properties of the neural populations. In neuroscience, we usually investigate the dynamic activity of

archetypal ensembles of neurons and their functional connectivity. It is generally assumed that functional and structural brain variables, such as the firing rates of individual neurons or the synchronous discharge of neural populations, have a bell-shaped input distribution [24–26]. That is, the variables describing functional and structural parameters of the brain are assumed to follow a normal distribution. This kind of statistic is based on the symmetry and normality; however, cognitive tasks, for example, can provide an important reshaping of the neural inputs.

At many physiological and anatomical levels, the distributions of the parameters follow arithmetic distributions, to a greater or lesser extent. The main issue is that most neurophysiological features of the brain are identified by strongly skewed distributions with heavy tails [18–23]. The skewed statistic is manifested through neural inputs that follow a non-Gaussian statistic as found in the olfactory bulb of flies [20] and also in the auditory cortex of mice [19]. This skewed statistic is also manifested in the response to a sensory stimulus such as light, touch, or sound that has been found to be proportional to the logarithm of stimulus amplitude [27–32]. Moreover the perception time and reaction time also change as the logarithm of the distance length, time interval, and even the decision-making and short-term memories follow this kind of statistic [33–35]. Thus, skewed distribution suggests a systematic general organization that allows the functional diversity within assemblies of neurons even if they are the same type of cell. That is to say, a neuronal population can be highly homogeneous, but for some particular conditions just a given subset of neurons could be activated by the meaningful inputs, causing skewed distributions [18–23].

Brain sensitivity to external inputs incorporates synaptic versatility so that neuronal reactions rely not only on synaptic plasticity but also on the behavioral states and the specific

<sup>\*</sup>fmontani@gmail.com

cognitive process, leading to skewed distributions [18–23]. Thus, the nonlinearity of input and output neural relationships can also transform the huge variability of the synaptic input into skewed distribution of firing rates [23]. This suggests that asymmetric distributions are fundamental to the structural and functional organization of the brain. Power-law and log-normal distributions are examples of asymmetric distributions. Both distributions are just a subset of heavily right skewed distributions. The justification for the use of the former is the appearance of scale-free phenomena, and the justification for the latter is the fact that such a distribution is the limit according to the central limit theorem for multiplicative processes, i.e., for the product of independent random variables [18,36].

Both types of distributions look very similar in a log-log graph, particularly in the tail zone. Thus, many times using one or the other to adjust the experimental data ends up being related to the measurement resolution of the specific section of the data, where both distributions have very different conformations, and to the previous hypothesis about the phenomenon under study following a skewed distribution [18–23]. Beyond the extensive experimental evidence about asymmetric distributions in sensory and other mental phenomena [18–23], very little is known about the process that gives rise to such distributions and the effect they have on a population of neurons. As is well known in physics, the appearance or disappearance of symmetries is related to the phase transitions in a system [37].

The main purpose of this work is to develop a neuronal modeling in order to investigate how skewed distributions affect the different levels of organizational activity in the brain dynamics. In the functional networks of the brain, the neurons in the cortex that are connected by strong synapses give rise to rapid firing bursts. Moreover, areas that are interconnected by weaker synapses have slower dynamics and they can contribute to produce a significant skewness in the distribution of inputs [18–23]. Thus, brain computations depend upon how neurons remodel inputs to spike outputs [37,38].

To decipher input-output transformation in cortical networks, we have to take into account that neuronal inputs can be characterized by strongly skewed distributions [18–23]. These skewed distributions have asymmetric alterations and heavy tails that cannot be modeled by bell-shaped distributions. Information in neural populations is often encoded in the activity of highly interconnected neural inputs that follow skewed statistics, so neural populations show higher order correlations in both their inputs and outputs due to intrinsic mechanisms of the neural circuits [18–22]. Despite extensive evidence of skewed distributions in the brain, very little is known about the origin of the cortical circuits and brain mechanisms that give rise to such distributions.

In this paper, we provide a complex system approach to understand the theoretical basis of the brain skewed distributions, in order to identify their implications for information processing. We introduce a model capable of generating spike trains by thresholding a multivariate skew distribution in their inputs. In order to do it, we use a recent extension of a multivariate distribution that has a parameter corresponding to the asymmetry of a skewed distribution [39–44] to take into account the heterogeneity of the neuronal synaptic inputs. The

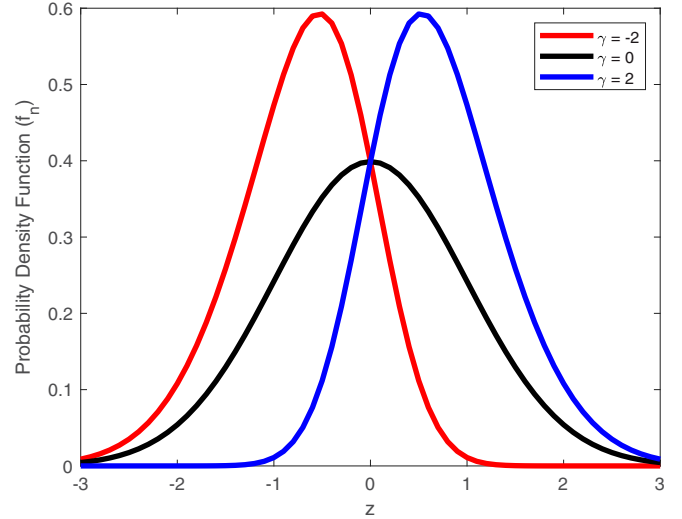


FIG. 1. Univariate closed skew-normal distribution for mean  $\mu = 0$ , standard deviation  $\sigma = 1$ , and three values of skew parameter  $\gamma = -2, 0, 2$ .

aim of this work is to investigate, at the analytical level, how the effect of an asymmetry in the neuronal input distributions could establish the transition from a spontaneous silence to synchronous states in a population of neurons, improving the neural systems' ability to powerfully encode data over different scales.

## II. MULTIVARIATE SKEW-NORMAL DISTRIBUTIONS

The multivariate skew distribution used here is the one introduced in Refs. [39–44]. This distribution was conceived as a multidimensional extension of the skew-normal distribution [40], with the desirable property of closure under linear transformation. A continuous random vector  $Z$  is said to have a closed skew Gaussian distribution if its probability density function (PDF) is given by [39]

$$f_n(z; \mu, \Sigma, \Gamma) = \frac{\phi_n(z; \mu, \Sigma)}{\Phi_n(0; I + \Gamma \Sigma \Gamma^t)} \Phi_n(\Gamma(z - \mu)). \quad (1)$$

Here  $\mu \in \mathbb{R}^{n \times 1}$ ,  $I$  is the identity matrix,  $\Sigma$  is a positive definite matrix,  $\Gamma \in \mathbb{R}^{n \times n}$ ,  $\phi_n(\cdot; \mu, \Sigma)$ , and  $\Phi_n(\cdot; \Sigma)$  denote the PDF and cumulative density function (CDF) of an  $n$ -dimensional normal distribution with mean  $\mu$  and covariance matrix  $\Sigma$  [39]. The superscript  $t$  denotes matrix transposition. In order to alleviate notation, we write  $\phi_n(\cdot; 0, I)$  as  $\phi_n(\cdot)$ , and  $\Phi_n(\cdot; 0, \Sigma)$  as  $\Phi_n(\cdot; \Sigma)$ . Thus, we denote the vector  $Z$  having the closed skew-normal (CSN) distribution:  $Z \sim \text{CSN}_n(\bar{\mu}, \Sigma, \Gamma)$ . Examples of univariate and bivariate distributions are plotted in Figs. 1 and 2, respectively.

There are two important properties of this distribution that we use. First, if we have a collection of  $n$  independent random variables with skew-normal distribution, then the joint distribution of the  $n$  random variables is CSN. Hence, the mutually independent case (i.i.d.) is given by  $\Sigma = \sigma^2 I$  and  $\Gamma = \gamma I$ . Second, if  $Y \sim \text{CSN}_n(\bar{\mu}, \Sigma, \Gamma)$ ,  $A$  is a constant nonsingular matrix of size  $n \times n$  and  $b \in \mathbb{R}^n$  is a constant vector, then

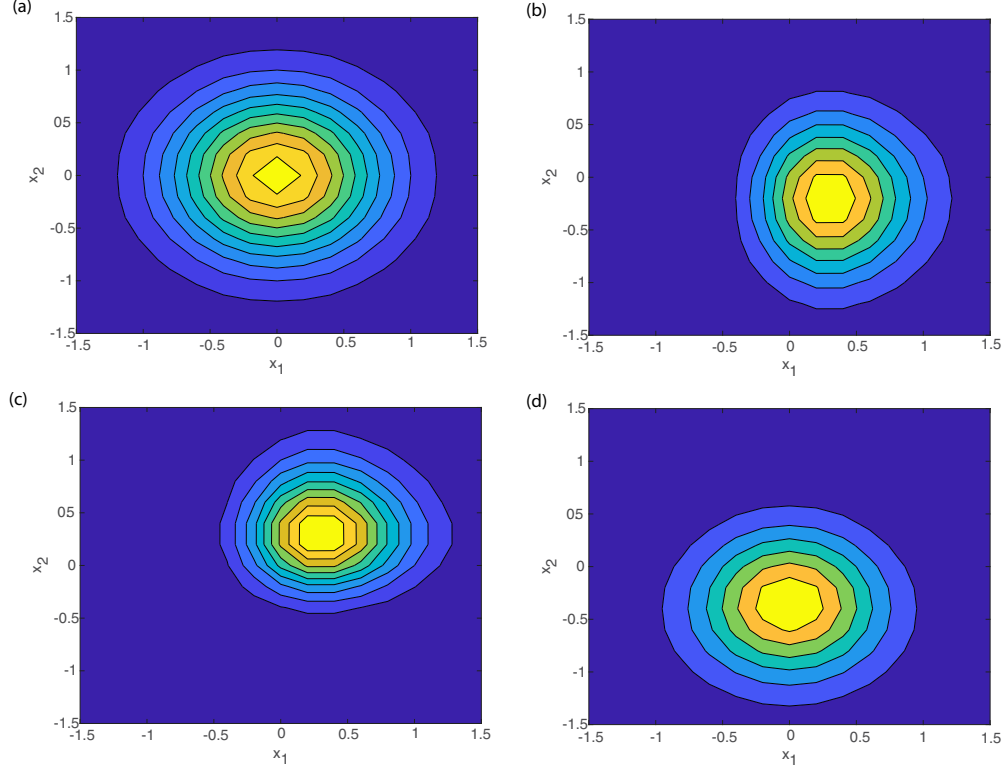


FIG. 2. Bivariate closed skew-normal distribution for mean  $\bar{\mu} = [0, 0]$ , standard deviation  $\Sigma = [0.3, 0; 0, 0.3]$ , and four values of skew matrix: (a)  $\Gamma = [0, 0; 0, 0]$ , (b)  $\Gamma = [3, 0; 0, -1]$ , (c)  $\Gamma = [0, 3; 3, 0]$ , and (d)  $\Gamma = [1, -1; -1, -1]$ .

$AY + b \sim \text{CSN}_n(b + A\bar{\mu}, A\Sigma A^t, \Gamma A)$ . This last property is the closure under linear transformations [39–44].

### III. SKEWED DICHOTOMIZED MODEL

Based on the recent findings in Refs. [18–23], we assume that the inputs  $Z$  are CSN distributions. Thus, we define a latent variable  $Z$  that obeys the closed skew-normal distribution [39–44] that would be considered the common inputs to all neurons in the population. The variable  $Z$  satisfies  $Z \in \mathbb{R}^{n \times 1}$ . Let us consider an  $n$ -dimensional binary random variable  $X \in \{0, 1\}^n$ , we set the spiking outputs ( $X = 1$ ) if and only if  $Z > 0$ , and silent ( $X = 0$ ) otherwise. Following the definition and properties of the closed skew-normal distribution [39,41–44], we can approximate  $Z$  as

$$Z \sim \text{CSN}_n(\bar{\mu}, \Sigma, \Gamma), \quad (2)$$

where the subscript  $n$  means that the dimensions of the variable  $Z$  are equal to the number of neurons in the pool,  $n$ . In addition,  $\bar{\mu}$  is the vector of means,  $\mu \in \mathbb{R}^{n \times 1}$ ,  $\Sigma$  is the matrix related to the covariance of the normal distribution, and  $\Gamma$  is a matrix related to the asymmetry of the distribution. If we have a collection of  $n$  independent random variables with skew-normal distribution, then the joint distribution of the  $n$  random variables is a closed skew-normal distribution [39,41–44]. Thus,  $\Sigma = \sigma^2 I$  and  $\Gamma = \gamma I$  give us the i.i.d. case, where  $I$  is the  $n \times n$  identity matrix and  $\sigma, \gamma \in \mathbb{R}$ . By the property of closure under linear transformations of the CSN, we can write

the variable  $Z$  as a sum as follows:

$$Z = \bar{\mu} + \sqrt{1 - \lambda} \Upsilon + \sqrt{\lambda} S e_n, \quad (3)$$

where  $\Upsilon \sim \text{CSN}_n(0, \sigma_1^2 I, \gamma_1 I) \in \mathbb{R}^{n \times 1}$ , so every  $\Upsilon_i \sim \text{CSN}_1(0, \sigma_1^2, \gamma_1)$ , and  $S \sim \text{CSN}_1(\sigma_2^2, \gamma_2) \in \mathbb{R}$ .  $e_n$  is a vector in  $\mathbb{R}^{n \times 1}$ , and  $\sigma_1, \sigma_2, \gamma_1, \gamma_2, \lambda \in \mathbb{R}$ . The variable  $\sqrt{\lambda} S$  follows the distribution  $\text{CSN}_1(0, \lambda \sigma_2^2, \frac{\gamma_2}{\sqrt{\lambda}})$ .

For simplicity, but without losing generality, we choose  $\sigma_1 = \sigma_2 = 1$ .

Here,  $\Upsilon_i$  is a closed skew Gaussian random variable (with unit variance) which is independent for each neuron (i.e., the independent input),  $S$  is a closed skew Gaussian random variable that is the common input to all neurons, and  $\bar{\mu}$  is a constant term giving the mean input. So, by controlling the parameters  $\lambda$  and  $\gamma$  of our model, we are balancing the terms corresponding to the independent [second term in Eq. (3)] or dependent [third term in Eq. (3)] inputs to the neurons. It is important to emphasize that the correlations in the activity of these neurons are due to the common input rather than due to physical connections between them. In some sense, we are modeling a layer of neurons that are receiving some common input from another layer or area. Despite that apparent simplicity, a recent study, analytically and numerically demonstrated the strong connection between the collective dynamics produced by the integrate-and-fire neuronal network and dichotomized models, and showed that the latter is an accurate model of the former, when modeling the effect of inputs on the firing statistics of these models [45].

Let us start with the calculation of the asymptotic firing rate distribution [24,25,46]. To do this, let us consider the probability  $P_{\text{SDG}}(X = x)$  of having a population binary vector  $X = x$ , where SDG stands for skew dichotomized Gaussian (SDG). Because we are considering a neuron pool,  $P_{\text{SDG}}(X = x)$  is only dependent on the number of firing neurons, i.e.,  $\|x\| = \sum_{i=1}^n x_i$ , where  $n$  is the number of neurons. In the case of finite  $n$ , we have

$$P_{\text{SDG}}(X = x) = \int_z P(X = x|z)p(z)dz \quad (4)$$

$$= \int_{-\infty}^{\infty} p_{\sqrt{\lambda}S}(s') \prod_{i=1}^n P(X_i = x_i|s') ds' \quad (5)$$

$$= \int_{-\infty}^{\infty} p_{\sqrt{\lambda}S}(s') \prod_{i=1}^n [1 - L(s')]^{1-x_i} L(s')^{x_i} ds', \quad (6)$$

where  $L(s') = P(Z_i > 0|s') = P(\Upsilon_i > -\frac{s'+\mu}{\sqrt{1-\lambda}}) = 1 - P(\Upsilon_i < -\frac{s'+\mu}{\sqrt{1-\lambda}}) = 1 - \text{CDF}_{\Upsilon_i}(-\frac{s'+\mu}{\sqrt{1-\lambda}})$ . Here  $\text{CDF}_{\Upsilon_i}(\cdot)$  means the cumulative density function for the random variable  $\Upsilon_i$ , and  $p_{\sqrt{\lambda}S}$  means the PDF for the unidimensional random variable  $\sqrt{\lambda}S$  in Eq. (3). The first line, Eq. (4), is obtained using the chain rule for probabilities. Equation (5) is obtained by replacing Eq. (3) and considering that  $\Upsilon$  is composed by independent variables  $\Upsilon_i$ , and the last line, Eq. (6), comes from the fact that  $x_i$  are binary variables [24,25,46].

In this case, the  $\text{CSN}_1$  reduces to the Azzallini and Dalla Valle's skew normal  $SN$  [40]. In order to keep all the asymmetry effects in only one parameter  $\gamma$ , we fix  $\gamma_1 = 0$ . In such case  $\Upsilon_i \sim N(0, 1)$ . Remembering that the population behavior is determined by the number of spiking neurons  $k = \|x\| = \sum_{i=1}^n x_i$  and that we are dealing with a pool of neurons (i.e., all are identical [24]), we can find the distribution of spikes:

$$P_{\text{SDG}}(K = k) = \quad (7)$$

$$= \binom{n}{k} P_{\text{SDG}}(X = x, \text{ where } \|x\| = k) \quad (8)$$

$$= \binom{n}{k} \int_{-\infty}^{\infty} p_{\sqrt{\lambda}S}(s') [1 - L(s')]^{n-k} L(s')^k ds' \quad (9)$$

$$= \binom{n}{k} Q_{\text{SDG}}(k). \quad (10)$$

By defining the normalized firing rate  $r = \frac{k}{n}$ , we could put  $U(s') = r \log L(s') + (1-r) \log(1-L(s'))$ , in order to have

$$Q_{\text{SDG}}(k) = \int_{-\infty}^{\infty} p_{\sqrt{\lambda}S}(s') \exp(nU(s')) ds'. \quad (11)$$

Thus, in the limit of large  $n$ , we can make a saddle-point approximation [47] and obtain

$$Q_{\text{SDG}}(k) \approx \sqrt{\frac{2\pi}{-nU''(s'_0)}} p_{\sqrt{\lambda}S}(s'_0) \exp(nU(s'_0)). \quad (12)$$

Here,  $L(s'_0) = r$  is the maximum of the function  $L(s')$ . So,  $1 - \Phi(-\frac{s'_0+\mu}{\sqrt{1-\lambda}}) = r$ , with  $\Phi$  being the cumulative of the standard normal distribution. From here, we can obtain the value  $s'_0 = -\sqrt{1-\lambda} \Phi^{-1}(1-r) - \mu = \sqrt{1-\lambda} \Phi^{-1}(r) - \mu$ . Also, we have  $U''(s'_0) = -\frac{L'(s'_0)^2}{r(1-r)}$ , and

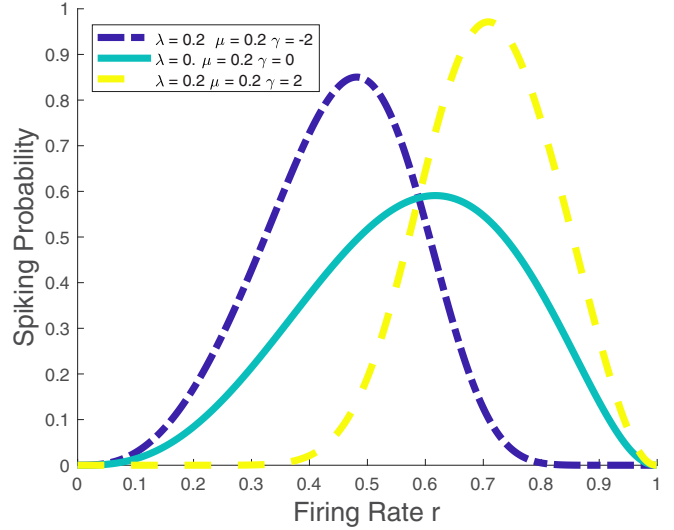


FIG. 3. Spiking probability for  $\lambda = 0.2$ ,  $\gamma = -2$  (blue dashed line),  $\gamma = 0$  (light blue line),  $\gamma = 2$  (yellow dashed line), and  $\mu = 0.2$ . We can observe that the skewness parameter, as expected, favors the states with more or less firing, depending on the sign of  $\gamma$ .

$\exp(nU(s'_0)) = [r^r(1-r)^{1-r}]^n$ . Moreover, we can determine that  $L'(s'_0) = \frac{1}{\sqrt{1-\lambda}} \phi(-\frac{s'_0+\mu}{\sqrt{1-\lambda}})$ , with  $\phi$  being the PDF of a standard normal distribution. Putting all together, we have

$$Q_{\text{SDG}}(k) = \sqrt{\frac{2\pi r(r-1)(1-\lambda)}{n}} \frac{p_{\sqrt{\lambda}S}(s'_0)}{\phi(-\frac{s'_0+\mu}{\sqrt{1-\lambda}})}. \quad (13)$$

Recalling that  $\sqrt{\lambda}S \sim \text{CSN}_1(0, \lambda, \frac{\gamma_2}{\sqrt{\lambda}})$ , we have  $p_{\sqrt{\lambda}S}(s'_0) = \frac{2}{\sqrt{\lambda}} \phi(\frac{s'_0}{\sqrt{\lambda}}) \Phi(\frac{\gamma_2 s'_0}{\sqrt{\lambda}})$ , where  $\phi$  and  $\Phi$  are the PDF and CDF of the standard normal distribution respectively.

Now we can calculate the spike distribution  $P_{\text{SDG}}(K = k) = \binom{n}{k} Q_{\text{SDG}}(k)$ . Considering Stirling's approximation of the binomial coefficient,  $\binom{n}{k} \approx \sqrt{2\pi n} (\frac{n}{e})^n$ , we arrive at the asymptotic spike count distribution  $f(r) = P(k)/n$ , with  $r = k/n$ :

$$f(r) = 2\sqrt{\frac{1-\lambda}{\lambda}} \frac{\phi(s'_0/\sqrt{\lambda})}{\phi(v)} \Phi\left(\gamma_2 \frac{s'_0}{\sqrt{\lambda}}\right), \quad (14)$$

with  $v = \Phi^{-1}(r)$  and  $s'_0 = \sqrt{1-\lambda} v - \mu$ . Let us remark that although broadly speaking this result has some similarity to the one obtained for the nonskewed model [24–26,46], we have, however, included an important factor that takes into account the biased skewed distribution of the neuronal inputs and its asymmetric variations through the parameter  $\gamma$ . This factor considerably changes the behavior of the spiking probability, as depicted in Figs. 3 and 4. It can be seen that the skewness parameter favors the states of resting or synchronized firing, depending on its sign, positive or negative, respectively. In the case of a bimodal distribution, as in Fig. 4, the skewness parameter can widely favor one of the two possible states of the system, modifying the nonskewed model (light blue curve) and generating a more synchronized population, both for the simultaneous firing (dark blue curve) and for the silence (yellow dashed curve).

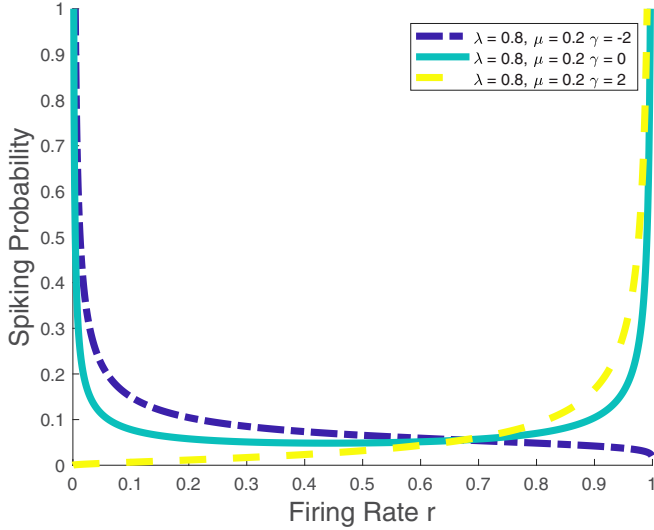


FIG. 4. Spiking probability for  $\lambda = 0.8$ ,  $\gamma = -2$  (blue line),  $\gamma = 0$  (light blue line),  $\gamma = 2$  (yellow dashed line), and  $\mu = 0.2$ . We can observe that the skewness parameter, as expected, favors the states of rest or firing, depending on the sign of  $\gamma$ .

We can also observe the firing behavior of the population on the raster plots in Fig. 5. Thus, we directly simulate the model by sampling  $n$  values of a skew-Gaussian distribution, and we threshold them. If the sampled values are greater than zero, the neuron fires, and it is plotted as a point on the corresponding row. This procedure is repeated for each time step, which corresponds to each column on the raster plot. It is observed that the increase in  $\gamma$  causes the population to move from a state in which many neurons are inactive, for  $\gamma = -1.9$ , to a pattern where the neurons fire synchronously, for  $\gamma = 1.9$ . Let us remark from Fig. 4 that in the nonskewed model (i.e., with  $\gamma = 0$ ), this distribution is bimodal as in Refs. [25,26,46]. However, if  $\gamma \neq 0$  it can greatly favor one of the system states, either firing or silence, depending on the sign of the skewness parameter.

**IV. TEMPERATURE DEPENDENCE OF THE MODEL**

First of all, let us rewrite the asymptotic spike count distribution  $f(r)$  as

$$f(r) = \frac{1}{Z_{SDG}} \exp\left(-\frac{1}{2} \frac{(1 - 2\lambda)(v - \frac{\mu\sqrt{1-\lambda}}{1-2\lambda})^2}{\lambda}\right), \quad (15)$$

with  $Z_{SDG} = \frac{1}{2\Phi(\frac{v}{\sqrt{\lambda}}(v\sqrt{1-\lambda}-\mu))} \exp(-\frac{\mu^2}{2(1-2\lambda)})\sqrt{\frac{\lambda}{1-\lambda}}$ . Here,  $v = \Phi^{-1}(r)$ .

Let us write the distribution for any model as  $P(x)$  with the temperature dependence  $T = 1/\beta$  as  $P_\beta(x) = \frac{P(x)^\beta}{Z_\beta}$  [25,26,48]. Considering that  $P(x) = \frac{P(k)}{\binom{n}{k}} = \frac{f(r)n}{\binom{n}{k}}$ , for large  $n$  the asymptotic distribution of firing at the temperature  $T = 1/\beta$  is  $f_\beta(r) = \frac{n}{Z_\beta} \exp(n(1-\beta)\eta(r))P(rn)^\beta$ , with  $Z_\beta$  being a normalization factor and  $\eta(r) = -r \log(r) - (1-r) \log(1-r)$ . The temperature here acts as a way of testing a direction in the parameter space of the possible models and is not a physical temperature; the aim is to see if there is anything

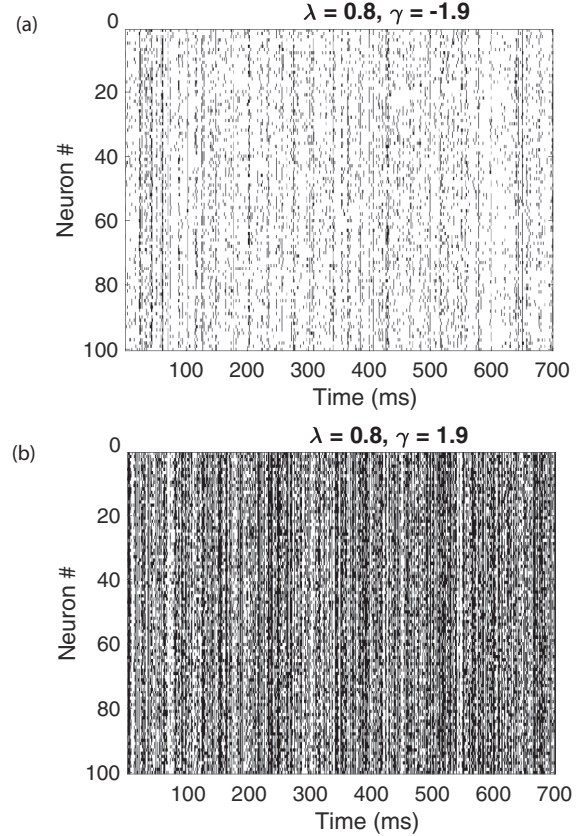


FIG. 5. Raster plot for (a)  $\gamma = -1.9$  and (b)  $\gamma = 1.9$ , with  $\lambda = 0.8$ ,  $\mu = 0.2$ . Each row represents a neuron, and each point represents a spike of the neuron. The effect of  $\gamma$  on the model is to modify the correlations.

special about the model (for  $T = 1$ , which would correspond to the critical one [25,26,48,49]). Figures 6 and 7 depict the spiking probabilities as a function of the firing rate  $r$  and there we can see the effect of the parameter  $\beta$  for two values of the input parameter,  $\lambda = 0.2$  and  $\lambda = 0.8$ , respectively. The temperature parameter then represents a global modification to correlations, and we need to explore the behavior of the model in relation to the  $\lambda$  and  $\gamma$  parameters.

The parameter  $\gamma$  acts as a control parameter. In the case of  $\beta < 1$ , from Figs. 6(a) and 7(a), we observe wide unimodal probability distributions. In this phase, we could say that the system is in a “disordered phase” when the temperature is near criticality with  $\beta < 1$ . In this case, it is very unlikely that the system is in extreme cases of synchronous firing or silence for the ensemble of neurons. Notice that Fig. 6(b) depicts unimodal probability distributions, when considering any value of  $\gamma$ . Figure 7(b) shows unimodal probability distributions for  $\gamma \neq 0$  and a bimodal distribution if  $\gamma = 0$ . We can see from Figs. 6(c) and 7(c) that at a temperature near criticality with  $\beta > 1$  and  $\gamma = 0$ , the probability distribution is bimodal with equal probability for the state of silence or synchronous firing, then there is a symmetry between these states. We can relate this region to an “ordered phase,” in which the system has a high probability of being in a state with all neurons in the same spiking condition. In addition, in the ordered phase, the skewness parameter  $\gamma$  breaks the symmetry between the

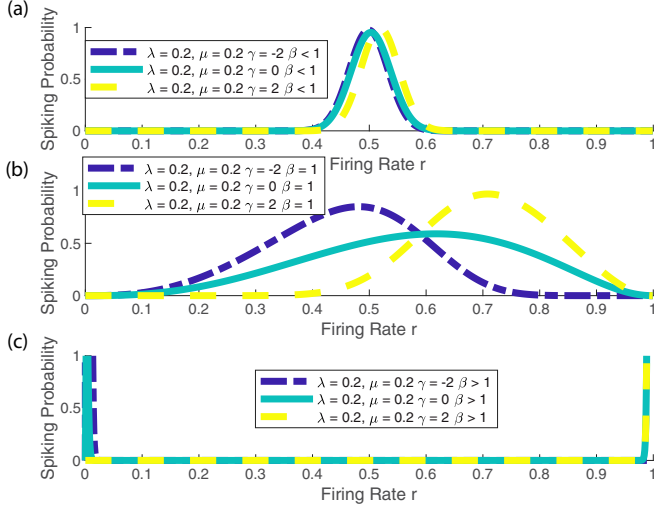


FIG. 6. Spiking probability versus the firing rate  $r$  considering the model with temperature dependence for  $\lambda = 0.2$ ,  $\gamma = -2, 0, 2$ , and  $\mu = 0.2$ . (a) Corresponds to a point near criticality with  $\beta < 1$ . (b) Considering the critical point  $\beta = 1$ . (c) Corresponds to a point near criticality with  $\beta > 1$ .

synchronous firing and quiescent state when the temperature is near criticality with  $\beta > 1$  and when considering a change in the skewness from  $\gamma < 0$  to  $\gamma > 0$ .

We can characterize the behavior of the system as a function of temperature and the number of neurons by calculating the entropy rate and the specific heat [25]:

$$s_\beta = \int_0^1 f_\beta(r) \eta(r) dr, \quad (16)$$

$$c_\beta = n \int_0^1 f_\beta(r) [\eta(r) - s_\beta]^2 dr. \quad (17)$$

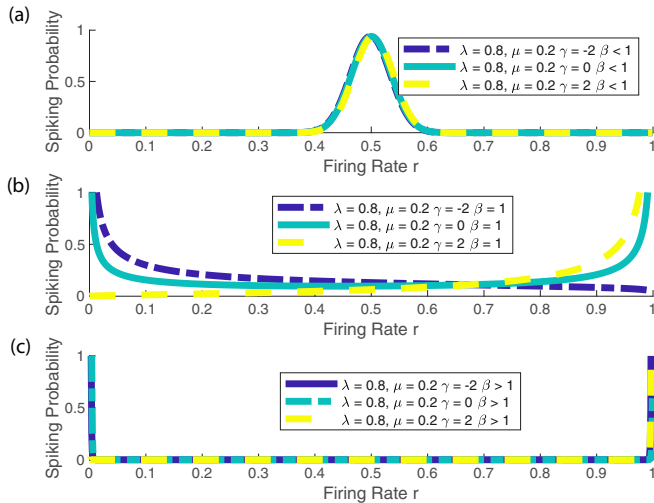


FIG. 7. Spiking probability vs the firing rate  $r$  considering the model with temperature for  $\lambda = 0.8$ ,  $\gamma = -2, 0, 2$ , and  $\mu = 0.2$ . (a) Corresponds to a point near criticality with  $\beta < 1$  (notice that the three curves overlap). (b) Considering critical point  $\beta = 1$ . (c) Corresponds to a point near criticality with  $\beta > 1$  (note that for  $\gamma = -2$  the population is silent, while for  $\gamma = 2$  the population is firing synchronously).

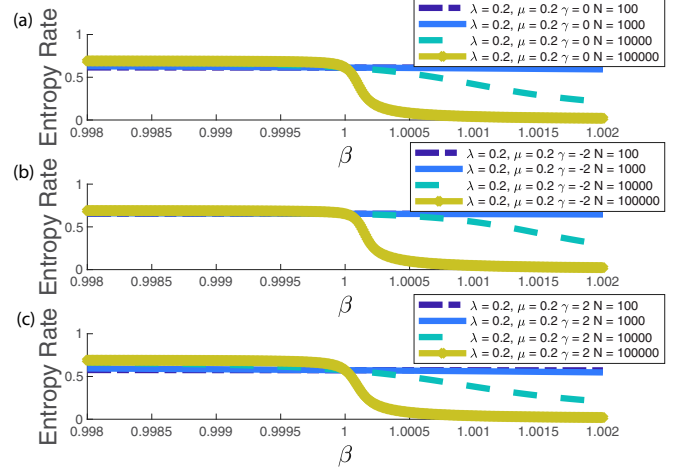


FIG. 8. Entropy rates as a function of  $\beta$  for  $\lambda = 0.2$ ,  $\gamma = -2, 0, 2$ , and considering  $N = 100, 1000, 10\,000, 100\,000$  neurons. (a) Corresponds to a skewness parameter  $\gamma = 0$ . (b) Setting the skewness  $\gamma = -2$ . (c) Corresponds to  $\gamma = 2$ .

Figures 8 and 9 show the entropy rates as a function of  $\beta$ , for  $\lambda = 0.2$  and  $\lambda = 0.8$ , respectively. The entropy rates are shown for three different values of  $\gamma = -2, \gamma = 0, \gamma = 2$ , and for several population sizes ( $N = 100, 1000, 10\,000, 100\,000$ ). It can be seen that for very large population sizes, the effect of the skewness parameter  $\gamma$  on the entropy rate is not significant; however, a transition point can be appreciated as the temperature approaches the critical one ( $\beta = 1$ ).

Specific heat as a function of  $\beta$  is shown in Figs. 10 and 11. Figure 10 shows that the effect of the skewness parameter is to slightly shift its maximum. It is observed from Figs. 10 and 11 that the effect of the parameter becomes more significant over the critical temperature and with a smaller number of neurons. When considering  $\beta = 1$  and  $\gamma = 0$ , our current formalism

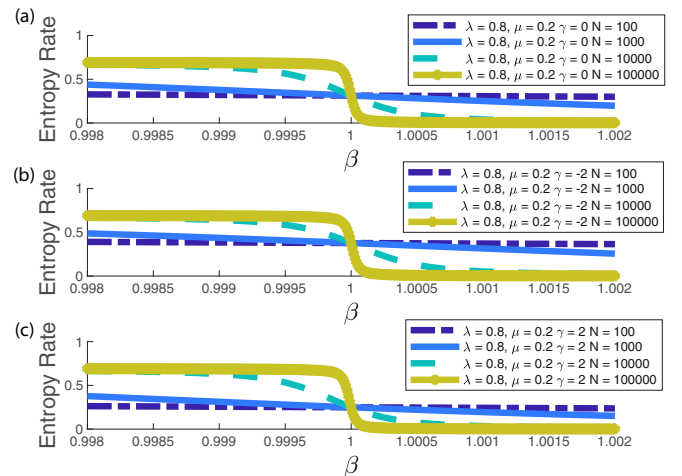


FIG. 9. Entropy rates as a function of  $\beta$  for  $\lambda = 0.8$ ,  $\gamma = -2, 0, 2$ , and considering  $N = 100, 1000, 10\,000, 100\,000$  neurons. (a) Corresponds to a skewness parameter  $\gamma = 0$ . (b) Setting the skewness  $\gamma = -2$ . (c) Corresponds to  $\gamma = 2$ .

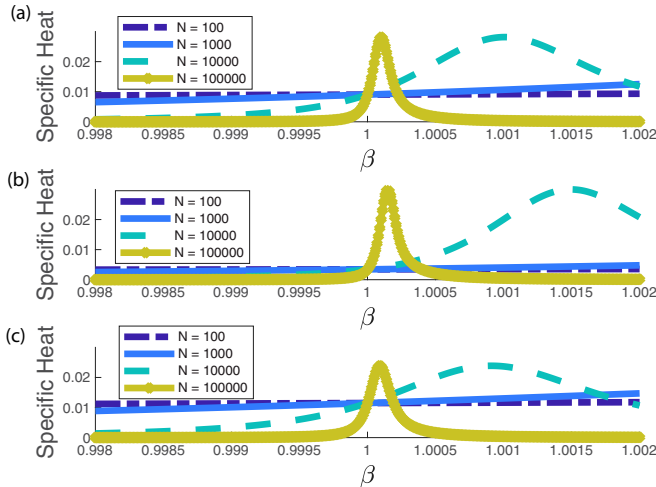


FIG. 10. Specific heat as a function of  $\beta$  for  $\lambda = 0.2$ ,  $\mu = 0.2$ , and considering  $N = 100, 1000, 10000, 100000$  neurons. (a) Corresponds to a skewness parameter  $\gamma = 0$ . (b) Setting the skewness  $\gamma = -2$ . (c) Corresponds to  $\gamma = 2$ .

reduces to the one proposed in Refs. [24–26], and the system is at a critical point as in Refs. [24–26].

It is interesting to calculate the behavior with  $\gamma$  and  $\beta$  for the average firing rate  $\langle r \rangle_\beta = \int_0^1 f_\beta(r) r dr$ . The average firing rate versus the deformation parameter  $\gamma$  is presented in Figs. 12 and 13. Figures 12(a) and 13(a) show that when the temperature is near criticality with  $\beta < 1$ , the average firing rate is just slightly dependent on the skewness parameter. Let us point out, as depicted in Figs. 12(b) and 13(b), that at the critical temperature  $\beta = 1$  the system is not in a state of silence or full synchronous firing, but instead is more likely to be at an intermediate value. The current results are in agreement with the recent findings reported in Refs. [37,50]. Next, in order to show a more appropriate comparison with the findings of Refs. [37,50], we characterize the changes in

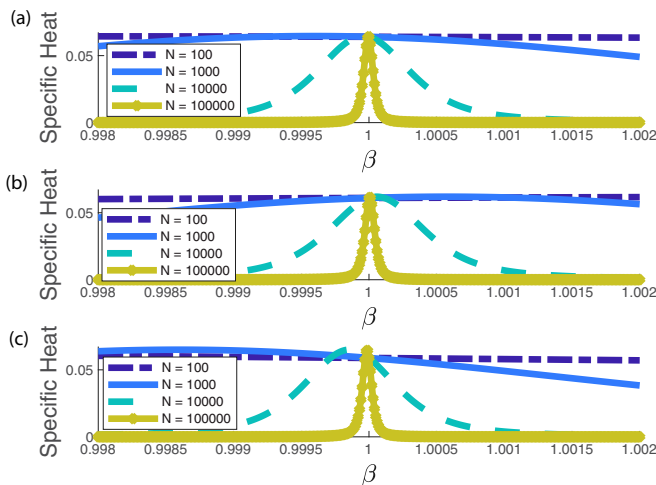


FIG. 11. Specific heat as a function of  $\beta$  for  $\lambda = 0.8$ ,  $\mu = 0.2$ , and considering  $N = 100, 1000, 10000, 100000$  neurons. (a) Corresponds to a skewness parameter  $\gamma = 0$ . (b) Setting the skewness  $\gamma = -2$ . (c) Corresponds to  $\gamma = 2$ .

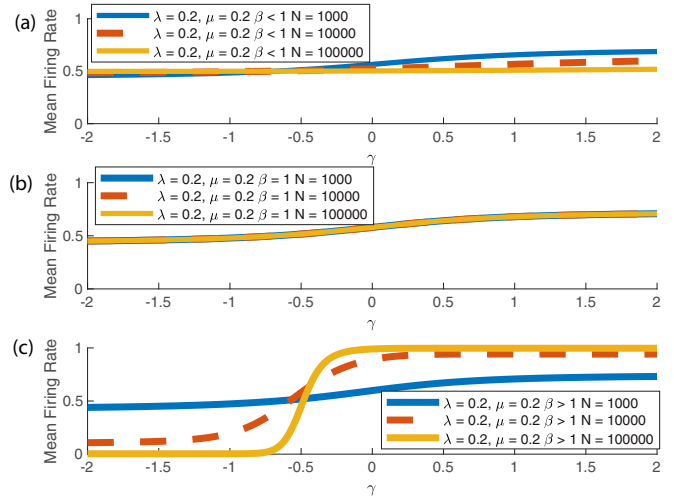


FIG. 12. Mean firing rate as a function of  $\gamma$  and considering  $N = 1000, 10000, 100000$  neurons,  $\mu = 0.2$  and  $\lambda = 0.2$ . (a) Corresponds to a point near criticality with  $\beta < 1$ . (b) Considering the critical point  $\beta = 1$ . (c) Corresponds to a point near criticality with  $\beta > 1$ .

the dynamics of the population states by using the standard deviation (Std) of the population firing rate. We choose to estimate standard deviations instead of calculating the coefficient of variation (CV) as in our current study we are not averaging over trials. It is important to emphasize that the Std is an accurate measure of synchronization. The Std of the population firing rate is calculated as  $\text{Std} = \int_0^1 (r - \langle r \rangle_\beta)^2 f_\beta(r)$ . Figure 14 and 15 depict Std versus  $\gamma$ , which shows the effect of the parameter  $\gamma$  for two values of the inputs parameter  $\lambda = 0.2$  and  $\lambda = 0.8$ , respectively. Larger values of Std correspond to more variability in the firing rate, showing that the system has more possibility of being in some synchronized or desynchronized state and highlighting that it is in an intermediate

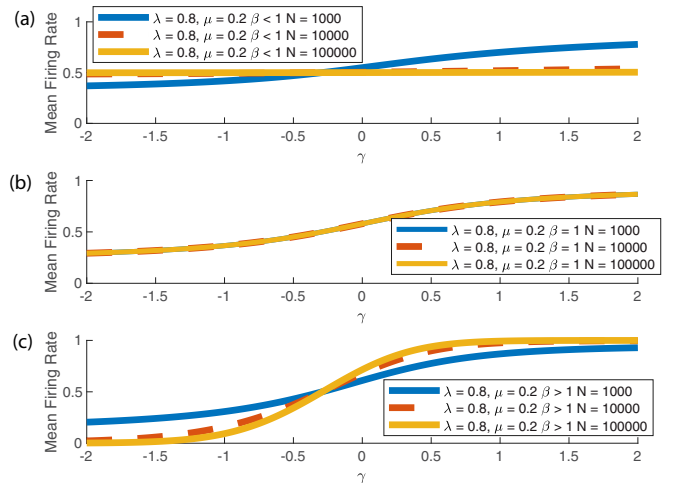


FIG. 13. Mean firing rate as a function of  $\gamma$ , considering  $N = 1000, 10000, 100000$  neurons,  $\mu = 0.2$  and  $\lambda = 0.8$ . (a) Corresponds to a point near criticality with  $\beta < 1$ . (b) Considering the critical point  $\beta = 1$ . (c) Corresponds to a point near criticality with  $\beta > 1$ .

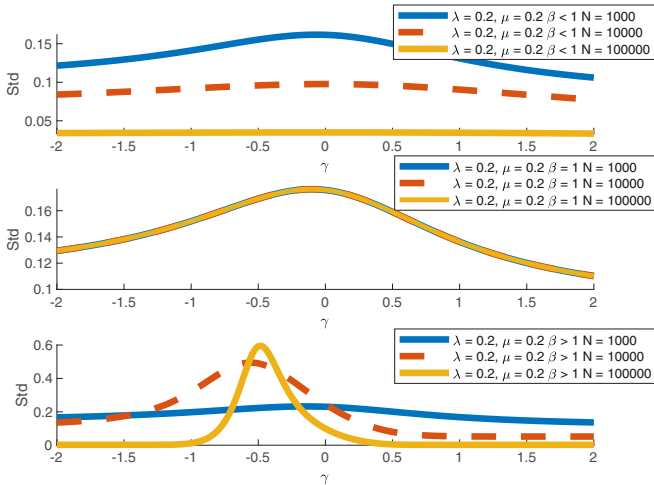


FIG. 14. The standard deviation (Std) as a function of  $\gamma$  and considering  $N = 1000, 10000, 100000$  neurons,  $\mu = 0.2$  and  $\lambda = 0.2$ . (a) Corresponds to a point near criticality with  $\beta < 1$ . (b) Considering the critical point  $\beta = 1$ . (c) Corresponds to a point near criticality with  $\beta > 1$ .

state between full synchronization and full desynchronization, as in Refs. [37,50]. Figures 14(a) and 15(a) show that as the temperature is below the critical one the synchronized states are significantly curtailed. Figures 14(b) and 15(b) allow us to determine that at the critical temperature  $\beta = 1$  the system is more likely to be at an intermediate value, instead of being at full synchronous firing (in agreement with the recent findings reported in Refs. [37,50]). That is, Figs. 14(c) and 15(c) show that the value of the Std peak increases by approximately a factor of 2 as the temperature goes from  $\beta = 1$  to  $\beta > 1$ . For the sake of completeness, we refer to the Appendix for

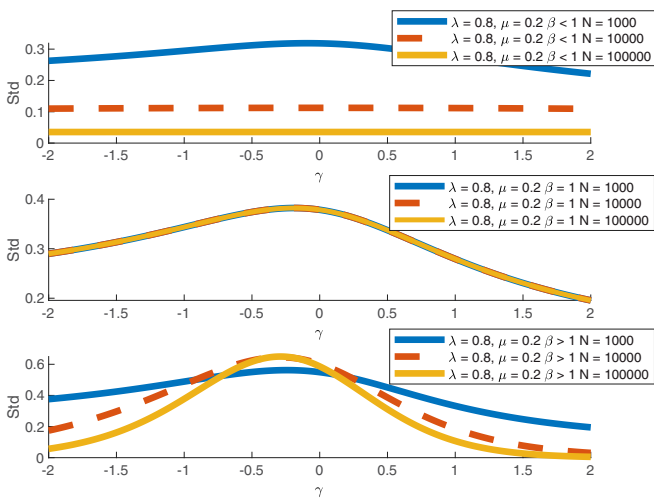


FIG. 15. The standard deviation (Std) as a function of  $\gamma$ , considering  $N = 1000, 10000, 100000$  neurons,  $\mu = 0.2$  and  $\lambda = 0.8$ . (a) Corresponds to a point near criticality with  $\beta < 1$ . (b) Considering the critical point  $\beta = 1$ . (c) Corresponds to a point near criticality with  $\beta > 1$ .

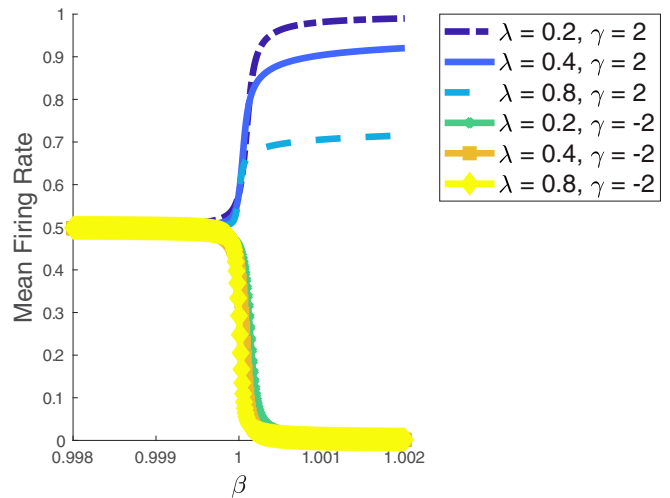


FIG. 16. Mean firing rate as a function of the temperature considering  $\gamma = -2$  and  $\gamma = 2$ , with  $\mu = 0.2$ .

details of the calculations of avalanche size distributions for parameters that present a power-law distribution (we use recent advanced tools developed in Ref. [51]).

In addition, as depicted in Figs. 12(c) and 13(c), when the temperature is near criticality with  $\beta > 1$ , we find that  $\gamma$  can highly enhance or weaken the firing of neurons, depending on the sign of  $\gamma$ . That is, for  $\gamma < 0$  the population is in a state of rest, while for  $\gamma > 0$  the system is in a synchronous state, with the majority of neurons firing, as seen in Figs. 12(c) and 13(c). That is, the effect of the skewness parameter is to change the dynamics of the population states by favoring one particular population state, either “fully excited” (with an average rate of firing close to one) or “fully inhibited” (with an average rate close to zero). Importantly, Figs. 12(c) and 13(c) depict that the effect of the parameter  $\gamma$  becomes more significant when considering a point near criticality with  $\beta > 1$ .

Summarizing, the effect of increasing the skewness parameter  $\gamma$  is to increase or decrease the firing rate. When  $\beta < 1$ , we observe that the average firing rate is quite independent of the skewness parameter. When  $\beta = 1$ , the system is much more likely to be at an intermediate firing state. But when  $\beta > 1$ , we find that  $\gamma$  can favor or impair the firing of neurons, depending on the sign of  $\gamma$ . For  $\gamma < 0$ , the population is in absolute silence, while for  $\gamma > 0$  the system is in a synchronous firing state, with the majority of neurons firing, as seen in Figs. 12(c) and 13(c). Note that the validity of these findings is confirmed through the Std estimations depicted in Figs. 14 and 15, as we showed that a phase transition occurs at an intermediate level of synchronization (in agreement with Refs. [37,50]).

Finally, Fig. 16 depicts the mean firing rate as a function of the temperature for two different skewness values,  $\gamma = -2$  and  $\gamma = 2$ , enhancing the behavior of the two states for the deformation parameter considered in the neuronal inputs and emphasizing that when the system is at critically ( $\beta = 1$ ) it is much more likely to be at an intermediate firing state as reported in Refs. [37,50].



## V. DISCUSSION AND CONCLUSIONS

Power-law and log-normal distributions are of fundamental importance in complex systems and neuroscience when investigating the statistical structure of the brain [18,21,22,37,52–55]. However, they are just a subset of heavily skewed distributions [41], and a more general framework may be desirable to accurately describe the dynamics of the brain.

In this work, we construct a formalism based on a model considering a biased skewed distribution in the inputs of a population of neurons to investigate the emergent properties of the neural ensembles. The model presented here can provide us with the neurocomputational basis to gain a better understanding of how the skewness in the inputs can change the dynamics at the output level. This can be useful for describing the nonlinear dynamics of neuronal populations more broadly.

Our results suggest that the asymmetry of the skewed distribution can induce a shift in the phase transition and we show how small changes in the neuron inputs due to the multi-layer structure of the neural networks, which follow a skewed distribution due to the slow activity of some neurons, can provide more plastic properties to the network dynamics, giving greater flexibility to the coding of neuronal information. That is, instead of simply reporting the mean parameter changes with a dichotomized Gaussian model [25,26,46], through the parameter  $\gamma$  related to the asymmetry of the distribution we can obtain accurate information that allows us to understand structural changes dependent on the synaptic plasticity of the inputs [18–23]. Input synapses can give rise to statistical dependences between groups of neurons larger than two, known as higher order interactions (HOIs) [37,52,53]. Importantly, higher order connection structures in the inputs have an essential role in understanding how neuronal avalanches process information in the brain [37,52,53].

Recent findings have shown substantial markers of criticality in the spiking activity in the mammalian cerebral cortex, and the critical point is not in the asynchronous ends or in the synchronous part of the system but rather at an intermediate value [37,50]. That is, although HOIs are ubiquitous in neuronal activity, the main dynamic characteristics of HOIs remain unknown.

Neuronal circuits can depict abrupt changes in their cortical states from period of sustained activity to quiescence states and the mechanisms behinds these transitions remains still unclear [56–58]. Conduction delay can induce “up and down states” in spiking neuronal systems [38,59] and also the slow activity of the neurons along with the simultaneous silences (“down states”), for specific time windows in the assemblies, help us understand the dynamics in higher order interactions in a simple way [60]. Simultaneous silences are related to weaker synapses that have slower dynamics and contribute to build the skewness in the input distributions [18–23]. Thus, weaker or stronger synapses give rise to different dynamics in the neuronal outputs [18–23]. Brain computations depend on how neurons transform inputs into spike outputs, and we take into account that the heterogeneity of neuronal inputs can be characterized by strongly skewed distributions.

The current formalism enables us to gain a better understanding of the role of inhibitory neurons in nonlinear network

rhythmic activity and in spontaneous activity between the “up state” and “down state” observed simultaneously in groups of neurons, a phenomenon of critical importance for working memory and attention [59]. Moreover, our current findings are in agreement with those of Refs. [37,50], as we show that when considering a biased skewed distribution in the inputs of a neural population, the critical point is not in the asynchronous ends or at the synchronous part of the system, but rather in an intermediate state. These findings are reinforced by Std estimations showing that at the critical point system is more likely to be at an intermediate state, and the Std peak increases by approximately twice its value as the temperature is above the critical temperature. This suggests that a phase transition occurs at an intermediate level of synchronization (as reported in Refs. [37,50]).

In this paper, we show that a simple change in the direction of bias of the skewed distribution in the neuronal inputs can induce a transition of states in the firing rate, passing spontaneously from silence (“down state”) to an absolute activity of action potentials (“up state”). This type of cortical dynamics between the up and down states occurs during slow-wave sleep, and therefore sleep is believed to be a mediator of mnemonic and homeostatic functions [61]. However, the mechanism by which this brain state can implement both the “selective” plasticity needed to consolidate new memory traces and the “general” plasticity needed to maintain a properly functioning neuronal system is not clear [62]. Recent findings suggest that both functions affect neurons differently based on their intrinsic speed of firing, so there is ubiquitous neuronal heterogeneity that generates skewed distributions in the neuronal inputs [61].

Our formalism considering a skewed distribution in neuronal inputs allows us to explain the intrinsic mechanisms that can lead to the consolidation of memory traces through a simple change in the bias of the distribution of neuronal inputs, which results in a transition from down state to up state. This type of formalism will allow us to capture the effects of the nonlinearity of the multiple dendritic spines, and in the near future this will be of help for understanding their possible implications on the temporal dependence of plasticity (STDP) when considering an assembly of neurons [63].

In this work, we investigate the neurocomputational mechanisms by which increased activity during slow oscillation acts to maintain network statistics, promoting a skewed distribution in the inputs and in neuronal firing rates and generating a transition from quiescent states to synchronous firing of the entire population of neurons [61]. This permits us to develop a theoretical framework to investigate the process by which spike activity during slow oscillation acts to maintain network statistics by promoting a skewed distribution of neuronal firing rates, and how a simple “perturbation” of that activity, which could occur, for example, by spike repetition, helps to integrate new memory traces through a transition between down state and up state in the existing cortical network.

Networks with skewed statistical properties have a wide dynamic range and provide stability, strength, and fault tolerance, and their energy efficiency can be very useful for brain circuits [64]. This is of particular interest as the synaptic inputs and spiking outputs follow skewed distributions, suggesting a systematic general organization that allows

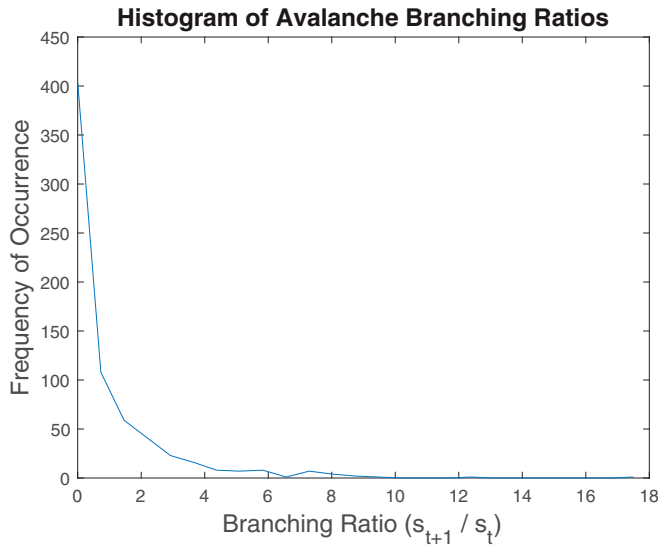


FIG. 17. The frequency of occurrence versus the branching ratio taking the same parameters as the ones taken in Fig. 5(a) with  $N = 50$ .

functional diversity within the assemblies of neurons even if they are the same type of cells [18–23]. This generates a way of understanding the applications of brain-machine interfaces, as a very robust synaptic force can produce disproportionately strong excitation across synapses, with high firing rates, while weak additional activity is more flexible in most synapses and can be crucial in improving the fidelity of spike transmission [18–23].

We think that the combination of the theoretical framework presented here, which takes into account a biased skewed distribution in the inputs of a neural population, and the recent experimental recording advances such as neuropixels [5–10] opens up a range of possibilities that would allow us to gain a better understanding of how information is transmitted in the brain.

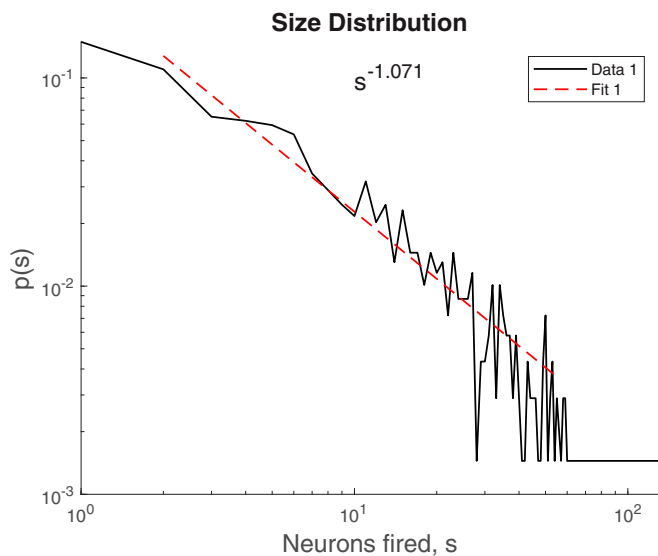


FIG. 18. Size distribution.  $p(s)$  vs neurons that fired. We take the same parameters as the ones taken in Fig. 5(a) with  $N = 50$ .

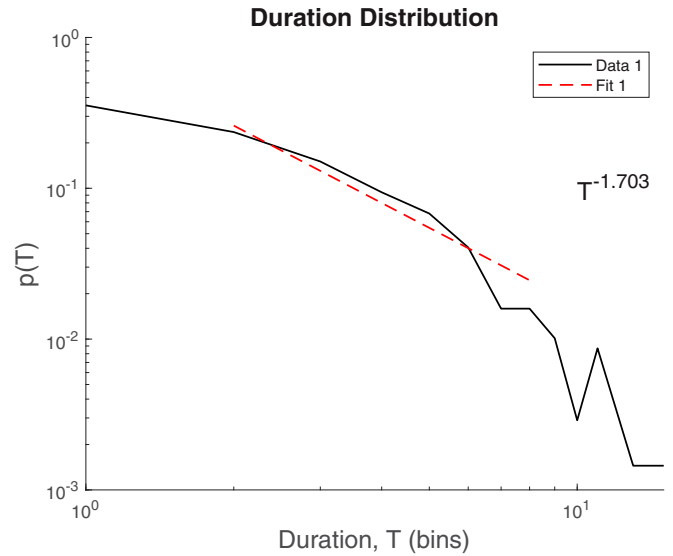


FIG. 19. Duration distribution.  $p(T)$  vs time bin ( $N = 50$ ). We take the same parameters as the ones taken in Fig. 5(a) with  $N = 50$ .

**ACKNOWLEDGMENTS**

We gratefully acknowledge funding from PUE 22920170100066CO IFLP-CONICET Argentina, PIP 11220130100327CO (2014/2016) CONICET, Argentina (F.M.), and Project No. 80120190100127LP Universidad Nacional de La Plata, Argentina.

**APPENDIX: POWER LAW FITTING**

In this Appendix, we use improved power-law fitting methodologies developed in Ref. [51] based upon previous advances [65,66] by utilizing an automated maximum likelihood estimation (MLE) technique to detect power law portions

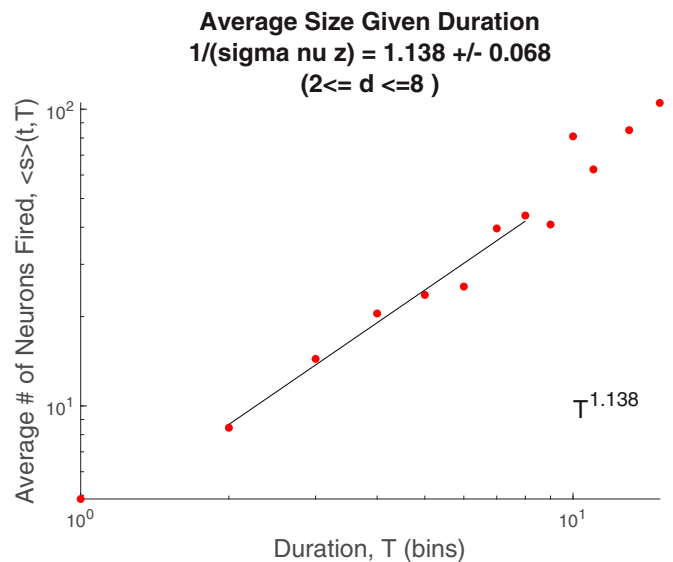


FIG. 20. The averaged number of neurons that fired vs the duration time (bins). We take the same parameters as the ones taken in Fig. 5(a) with  $N = 50$ .

of data histograms. Let us remark that the current approach can automatically control for data sets with subsampling bias in the tail of a power-law distribution. As the neural avalanches are usually highly subsampled, this improvement is particularly important in power law determination of neural avalanches. We perform then calculations of avalanche size distributions for parameters at the critical temperature ( $\beta = 1$  and  $\gamma < 0$ ) that presents a power law distribution. We determine avalanches using raster plots similar to the one presented in Fig. 5 of the main text.

Figure 17 depicts the histogram of the avalanche branching ratio, that is, the frequency of occurrence versus the branching

ratio. Note that Fig. 18 shows the estimation of avalanche size distributions versus the neurons that fired. Figure 19 shows the estimation of avalanches duration distributions versus the time bins. Finally, Fig. 20 present the averaged number of neurons that fired versus the duration time (bins). We can conclude that they present power law distribution at the critical temperature.

As part of a future work, we plan to investigate exhaustively the parameter space for the different power law distributions and log-like distributions around the critical point ( $\beta \neq 1$ ) that form the different subsets of heavily right skewed distributions.

- 
- [1] S. Royer, B. Zeman, M. Barbic, A. Losonczy, G. Buzsáki, and J. Magee, *Eur. J. Neurosci.* **31**, 2279 (2010).
- [2] K. Harris, R. Quiñero, J. Freeman, and S. Smith, *Nat. Neurosci.* **19**, 1165 (2016).
- [3] E. Trautmann, S. Stavisky, S. Lahiri, K. Ames, M. Kaufman, D. O’Shea, S. Vyas, X. Sun, S. Ryu, S. Ganguli, and K. Shenoy, *Neuron* **103**, 292 (2019).
- [4] G. Hong and C. Lieber, *Nat. Rev. Neurosci.* **20**, 330 (2019).
- [5] J. Abbott, T. Ye, K. Krenek, R. S. Gertner, S. Ban, Y. Kim, L. Qin, W. Wu, H. Park, and D. Ham, *Nat. Biomed. Eng.* **4**, 232 (2020).
- [6] J. Jun, N. Steinmetz, J. Siegle, D. Denman, M. Bauza, B. Barbarits, A. Lee, C. Anastassiou, A. Andrei, C. Aydin, M. Barbic, T. Blanche, V. Bonin, J. Couto, B. Dutta, S. Gratiy, D. Gutnisky, M. Häusser, B. Karsh, P. Ledochowitsch, C. Lopez, C. Mitelut, S. Musa, M. Okun, M. Pachitariu, J. Putzeys, P. Rich, C. Rossant, W. Sun, K. Svoboda, M. Carandini, K. Harris, C. Koch, J. O’Keefe, and T. Harris, *Nature (London)* **551**, 232 (2017).
- [7] J. Putzeys, B. Raducanu, A. Carton, J. De Ceulaer, B. Karsh, J. Siegle, N. Helleputte, T. Harris, B. Dutta, S. Musa, and C. Lopez, *IEEE Trans. Biomed. Circuits Syst.* **13**, 1635 (2019).
- [8] N. Steinmetz, C. Koch, K. Harris, and M. Carandini, *Curr. Opin. Neurobiol.* **50**, 92 (2018).
- [9] J. Chung, H. Joo, J. Fan, D. Liu, A. Barnett, S. Chen, C. Geaghan-Breiner, M. Karlsson, M. Karlsson, K. Lee, H. Liang, J. Magland, J. Pebbles, A. Tooker, L. Greengard, V. Tolosa, and L. Frank, *Neuron* **101**, 1 (2019).
- [10] R. Q. Quiroga, *Cell* **179**, 1015 (2019).
- [11] D. M. Zoltowski and J. Pillow, *Adv. Neural Inf. Process. Syst.* **31**, 3517 (2018).
- [12] I. Samengo and A. Treves, *Phys. Rev. E* **63**, 011910 (2000).
- [13] E. Castro, P. Polosecki, I. Rish, D. Pustina, J. Warner, A. Wood, G. Sampaio, and C. Cecchi, *NeuroImage: Clinical* **19**, 443 (2018).
- [14] C. Lynn and D. Bassett, *Nat. Rev. Phys.* **1**, 318 (2019).
- [15] C. W. Lynn, L. Papadopoulos, A. E. Kahn, and D. S. Bassett, *Nat. Phys.* **16**, 965 (2020).
- [16] M. Li, Y. Han, M. J. Aburn, M. Breakspear, R. A. Poldrack, J. M. Shine, and J. T. Lizier, *PLoS Comput. Biol.* **15**, e1006957 (2019).
- [17] J. Taghia, W. Cai, S. Ryali, J. Kochalka, J. Nicholas, T. Chen, and V. Menon, *Nat. Commun.* **9**, 2505 (2018).
- [18] G. Buzsáki and K. Mizuseki, *Nat. Rev. Neurosci.* **15**, 264 (2014).
- [19] M. DeWeese and A. Zador, *J. Neurosci.* **26**, 12206 (2006).
- [20] V. Bhandawat, S. R. Olsen, N. W. Gouwens, M. L. Schlieff, and R. I. Wilson, *Nat. Neurosci.* **10**, 1474 (2007).
- [21] K. Mizuseki and G. Buzsáki, *Cell Rep.* **4**, 1010 (2013).
- [22] G. Buzsáki, *Science* **347**, 612 (2015).
- [23] A. Roxin, N. Brunel, D. Hansel, G. Mongillo, and C. van Vreeswijk, *J. Neurosci.* **31**, 16217 (2011).
- [24] S. Amari, H. Nakahara, S. Wu, and Y. Sakai, *Neural Comput.* **15**, 127 (2003).
- [25] J. H. Macke, M. Opper, and M. Bethge, *Phys. Rev. Lett.* **106**, 208102 (2011).
- [26] J. Macke, A. Berens, P. Ecker, A. Tolias, and M. Bethge, *Neural Comput.* **21**, 397 (2009).
- [27] M. Muniak, S. Ray, S. Hsiao, J. Dammann, and S. Bensmaia, *J. Neurosci.* **27**, 11687 (2007).
- [28] J. Pardo-Vazquez, M. Castiñeiras-de Saa, J. R. Valente, I. Damião, T. Costa, M. Vicente, A. Mendonça, Z. Mainen, and A. Renart, *Nat. Neurosci.* **22**, 1493 (2019).
- [29] S. Bensmaia, *Behav. Brain Res.* **190**, 165 (2008).
- [30] J. Clemens, N. Ozeri-Engelhard, and M. Murthy, *Nat. Commun.* **9**, 134 (2018).
- [31] F. Montani, A. Oliynyk, and L. Fadiga, *Int. J. Neural Syst.* **27**, 1650009 (2017).
- [32] D. Drennan and E. Lalor, *eNeuro* **6**, 0082 (2019).
- [33] J. I. Gold and M. N. Shadlen, *Nature (London)* **404**, 390 (2000).
- [34] G. Deco and E. T. Rolls, *Eur. J. Neurosci.* **24**, 901 (2006).
- [35] I. Singh, Z. Tiganj, and M. Howard, *Neurobiol. Learn. Mem.* **153**, 104 (2018).
- [36] M. Berger, *Trans. Am. Math. Soc.* **285**, 777 (1984).
- [37] A. J. Fontenele, N. A. P. de Vasconcelos, T. Feliciano, L. A. A. Aguiar, C. Soares-Cunha, B. Coimbra, L. Dalla Porta, S. Ribeiro, A. J. Rodrigues, N. Sousa, P. V. Carelli, and M. Copelli, *Phys. Rev. Lett.* **122**, 208101 (2019).
- [38] P. M. Esir, S. Y. Gordleeva, A. Y. Simonov, A. N. Pisarchik, and V. B. Kazantsev, *Phys. Rev. E* **98**, 052401 (2018).
- [39] A. Gupta, G. González-Farías, and J. Domínguez-Molina, *J. Multivariate Anal.* **89**, 181 (2004).
- [40] A. Azzalini and A. Dalla Valle, *Biometrika* **83**, 715 (1996).
- [41] A. Azzalini, *Skew-Normal Family of Distributions* (J. Wiley and Sons, New York, 2015).

- [42] R. Arellano-Valle and A. Azzalini, *J. Multivariate Anal.* **99**, 1362 (2008).
- [43] A. Azzalini and A. Capitanio, *J. R. Stat. Soc.: Ser. B* **61**, 579 (1999).
- [44] A. Azzalini, *Scand. J. Stat.* **32**, 159 (2005).
- [45] D. A. Leen and E. Shea-Brown, *J. Math. Neurosci.* **5**, 17 (2015).
- [46] F. Montani, E. Phoka, M. Portesi, and S. Schultz, *Phys. A (Amsterdam, Neth.)* **392**, 3066 (2013).
- [47] R. Butler, *Saddlepoint Approximations with Applications*, Cambridge Series in Statistical and Probabilistic Mathematics (Cambridge University Press, Cambridge, UK, 2007).
- [48] G. Tkacik, E. Schneidman, M. Berry II, and W. Bialek, [arXiv:q-bio/0611072](https://arxiv.org/abs/0611072) (2006).
- [49] O. Kinouchi and M. Copelli, *Nat. Phys.* **2**, 348 (2006).
- [50] N. Lotfi, A. J. Fontenele, T. Feliciano, L. A. A. Aguiar, N. A. P. de Vasconcelos, C. Soares-Cunha, B. Coimbra, A. J. Rodrigues, N. Sousa, M. Copelli, and P. V. Carelli, *Phys. Rev. E* **102**, 012408 (2020).
- [51] N. Marshall, N. Timme, N. Bennett, M. Ripp, E. Lautzenhiser, and J. Beggs, *Front. Physiol.* **7**, 250 (2016).
- [52] S. Yu, H. Yang, H. Nakahara, G. S. Santos, D. Nikolić, and D. Plenz, *J. Neurosci.* **31**, 17514 (2011).
- [53] L. Montangie and F. Montani, *Phys. Rev. E* **94**, 042303 (2016).
- [54] L. Montangie and F. Montani, *Phys. A (Amsterdam, Neth.)* **471**, 845 (2017).
- [55] E. Balaguer-Ballester, R. Nogueira, J. M. Abofalia, R. Moreno-Bote, and M. V. Sanchez-Vives, *PLoS Comput. Biol.* **16**, e1007862 (2020).
- [56] T. Engel, N. Steinmetz, M. Gieselmann, A. Thiele, T. Moore, and K. Boahen, *Science* **354**, 1140 (2016).
- [57] D. Jercog, A. Roxin, P. Barthó, A. Luczak, A. Compte, and J. de la Rocha, *Elife* **6**, e22425 (2017).
- [58] J. Tukker, P. Beed, D. Schmitz, M. Larkum, and R. Sachdev, *Front. Syst. Neurosci.* **14**, 22 (2020).
- [59] D. Holcman and M. Tsodyks, *PLoS Comput. Biol.* **2**, e23 (2006).
- [60] H. Shimazaki, K. Sadeghi, T. Ishikawa, Y. Ikegaya, and T. Toyozumi, *Sci. Rep.* **5**, 9821 (2015).
- [61] D. Levenstein, B. O. Watson, J. Rinzel, and G. Buzsáki, *Curr. Opin. Neurobiol.* **44**, 34 (2017).
- [62] C. Lea-Carnall, N. Trujillo-Barreto, M. Montemurro, W. El-Deredy, and L. Parkes, *Proc. Natl. Acad. Sci. USA* **114**, 8871 (2017).
- [63] J. Gjorgjieva, C. Clopath, J. Audet, and J.-P. Pfister, *Proc. Natl. Acad. Sci. USA* **108**, 19383 (2011).
- [64] C. Torres-Huitzil and B. Girau, *IEEE Access* **5**, 17322 (2017).
- [65] A. Clauset, C. R. Shalizi, and M. E. J. Newman, *SIAM Rev.* **51**, 661 (2009).
- [66] A. Deluca and A. Corral, *Acta Geophys.* **61**, 1351 (2013).